Sensitivity analysis of the thermal performance of a parabolic trough concentrator using Al_2O_3 and SiO_2/Vegetable oil as heat transfer fluid

Venant Sorel Chara-Dackou [a,b,*], Donatien Njomo [a], René Tchinda [c], Yvon Simplice Kondji [b], Mahamat Hassane Babikir [d], Hermann Chopkap Noume [a], Boris Abeli Pekarou Pemi [a], Armel Zambou Kenfack [a], Ibrahim Ngapouth Mbouombouo [a]

[a] Department of Physics, Faculty of Science, University of Yaounde I, P.O. Box 812, Yaounde, Cameroon
[b] Carnot Energy Laboratory (CEL), Department of Physics, Faculty of Science, University of Bangui, P.O. Box 1450, Bangui, Central African Republic
[c] University Institute of Technology Fotso Victor of Bandjoun, University of Dschang, Cameroon
[d] Department of Physics, University of N'djamena, P.O. Box 1117, N'Djamena, Chad

A R T I C L E   I N F O

A B S T R A C T

This paper aims to highlight the use of different heat transfer fluid (HTF) configurations based on vegetable oils in Parabolic Trough Solar Concentrator (PTSC). Rapeseed and jatropha oils as innovative heat transfer materials combined with SiO_2 and Al_2O_3 to obtain six (6) HTF configurations are used in a 1-dimensional PTSC model. The thermophysical properties of the nanofluids are determined from correlations derived from the literature, using Gauss-Seidel method from a numerical code developed in Matlab software. Model validation is obtained. Thermal sensitivity analysis shows that the use of rapeseed increases the thermal efficiency of the PTSC by around 4.21 % compared with jatropha. The use of nanofluids reduces thermal losses within the system due to thermal gradients. For a fixed irradiance and each 1 %–4 % increase in volume fraction, thermal efficiency increases by around 1.96 % when Al_2O_3/rapeseed is used and by 0.47 % when SiO_2/rapeseed is used compared with rapeseed. Similarly, thermal efficiency increases by around 1.98 % when Al_2O_3/jatropha is used and decreases by around 0.20 % when SiO_2/jatropha is used compared with jatropha. However, the positive effects of nanoparticles on thermal conductivity alone are not always sufficient to improve thermal efficiency, and thermal effects on heat capacity should also be considered.

1. Introduction

In today's dynamic world of socio-economic and environmental challenges, energy conversion, conservation and utilization systems are the subject of much controversy in scientific and related fields [1–6]. The PTSC, known as one of the world's leading energy conversion systems, offers multitudes of possibilities for the efficient conversion, management, production and use of solar energy [7, 8]. The HTF is one of the essential elements of PTSC in its various energy production processes [9–11]. It plays an essential role in the

---

* Corresponding author. Department of Physics, Faculty of Science, University of Yaounde I, P.O. Box 812, Yaounde, Cameroon.
  E-mail address: chav7@yahoo.com (V.S. Chara-Dackou).

quality and quantity of its thermal performance. The choice of fluids to be used in PTSCs as transfer fluids is based on criteria such as high thermal conductivity and thermal capacity, availability in industrial quantities, low cost, acceptable ecobalance, thermal compatibility with contact materials, low toxicity and others [12]. Odeh et al. [13] used water and Syltherm 800 oil to generate steam directly from a PTSC. Analyses showed that using water as HTF reduces heat loss with a lower heat loss coefficient than Syltherm 800 as HTF. Forristall [14] using Xceltherm 600, Therminol VP-1, 60-40 salt, Syltherm 800 and Hitec XL salt as HTF in a PTSC found that highest value of thermal efficiency is obtained when Syltherm 800 and Xceltherm 600 are used. Moreover, these fluids aren't relatively cheaper. In their comparative analysis of molten salt, water and thermal oil as HTF in a PTSC, Montes et al. [15] found that optimum system efficiency is achieved using water. Ouagued and Khellaf [16] used Syltherm XLT, Syltherm 800, Marlotherm X Santotherm 59 and Therminol D12 in their numerical simulation of temperatures and heat gains. The results showed that Syltherm 800 can be used at temperatures above 427 °C, while Syltherm XLT and Marlotherm X can only be used at temperatures below 427 °C. The other HTFs can be used between 377 °C and 477 °C. In this same order of comparative studies of HTFs on improving the thermal performance of PTSCs, we can cite the experimental work of Wang et al. [17] who show that the use of molten salt generates high pressure losses and low thermal efficiency, Tahtah et al. [18], who show a rapid increase in outlet temperature evaluation when using as HTF thermal oil compared with water, and the numerical work of Babikir et al. [19], who show that the best thermal efficiency is obtained when using Therminol 66 as HTF compared with Therminol VP-1 and treated and untreated water. These reviewed works show the good performance of synthetic oils relative to water, but at a lower cost than water. These HTFs, commonly referred to as conventional or traditional fluids, have shown their advantages according to the above-mentioned criteria, but also have limitations with direct effects on the thermal performance of PTSCs, such as low thermal conductivity. The use of nanoparticles in base fluids has emerged as a technique for improving their thermophysical properties, hence the interest in nanofluids [20]. Sokhansefat et al. [21] used nanofluid Al_2O_3/Synthetic oil to improve heat transfer in the absorber tube of a PTSC. The results showed that the heat transfer coefficient (HTC) increased with increasing particle fraction ranging from 1 %, 3 % and 5 %. Paul et al. [22] using Al_2O_3/ionic liquid analyzed the thermal performance of a concentrated solar power (CSP) with volume fractions of 0.18 %, 0.36 % and 0.9 %. It was found that for a volume fraction of 0.9 % the thermal conductivity increased by 11 % and the thermal heat capacity by 49 %. Mwesigye et al. [23] in thermodynamic optimization of PTSC receiver performance using Al_2O_3/Synthetic oil with volume fraction variation of 0–4%, 0–6% and 0–8% observed an increase in heat transfer performance of 35 %, 54 % and 76 % respectively. The maximum efficiency improvement was 7.6 % recorded at the lowest temperature and Reynolds number. Toghyani et al. [24] in their work on PTSCs using SiO_2, CuO, Al_2O_3 and TiO_2 with Therminol-55 and varying the volume fraction from 2 to 5.5 % showed that the enhancement in overall exergy efficiency was 6 %, 3 %, 11 % and 9 % when using these nanoparticles respectively. In analyzing the thermal performance of PTSC, Ghasemi and Ranjbar [25] using CuO, Al_2O_3 with water under uniform heat flux showed that by varying the volume fraction by 0.5 %, 1.5 % and 3 % the HTC improved up to 28 % for Al_2O_3 and 35 % for CuO at the volume fraction. Faizal et al. [26] in their study estimated that 10,239 kg, 8625 kg, 8857 kg and 8618 kg of the total weight for 1000 units of solar concentrators can be saved for CuO, SiO_2, TiO_2 and Al_2O_3 nanofluids respectively with base fluid water and that the use of nanofluids reduces the cost of environmental damage. Several other traditional fluids have been used with different types of nanoparticles whose variations in their volume fraction have shown positive enhancements in the thermal performance of PTSCs [27,28]. The example is that of Chakraborty et al. [29,30], who show maximum improvement in thermal efficiency and Nusselt number when using hybrid nanofluids (water, CuO and Al_2O_3) in
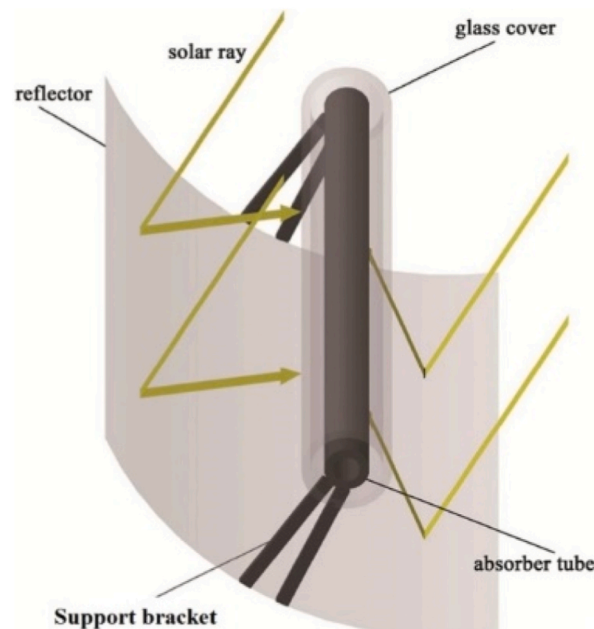

Fig. 1. Physical model of a PTSC with main elements [33].

different types of PTSC solar receivers. Also those of Ref. [31], using hybrid nanofluids in rotating receiver tubes with variable speeds showed improved values for outlet temperature and heat transfer coefficient. This work shows that nanoparticles can make a very significant contribution to improving the thermal performance of HTFs, but at a costly price. However, in the work by Hoffmann et al. [32], it was pointed out that vegetable oils are much cheaper, available on an industrial scale and offer very good thermal performance, including a good ecobalance, compared with synthetic oils. Referring to the work of Ref. [**32**], Chara-Dackou et al. [33] tested vegetable oils against the synthetic oil Therminol VP-1 and concluded that they can be used at high temperatures and also as a substitute for conventional HTFs in PTSCs. All this without a validation test of their performance and without, however, proposing an optimal condition for improving their thermal performance in PTSCs. What's more, none of the work cited in the literature has attempted to couple nanoparticles with vegetable oils such as HTF to analyze their thermal contribution to improving the thermal performance of PTSCs. Yet this could prove highly promising.

Thus, in a critical climatic and economic context, vegetable oils present themselves as a real asset in the solar industry as HTF for PTSC systems relative to the findings of Refs. [12,32] for sustainable energy production.

This study highlights a new thermal design based on the use of different heat transfer fluid (HTF) configurations based on vegetable oils combined with nanoparticles in PTSCs, in contrast to those generally used. A sensitivity analysis of the thermal effects of using vegetable oils and nanofluids as HTFs on the performance of the PTSC system derived from Ref. [33] is carried out from a quantitative and qualitative point of view. Two vegetable oils (jatropha and rapeseed) as base fluids and Al_2O_3 and SiO_2 nanoparticles are chosen to obtain six (6) HTFs configurations. A numerical code in Matlab has been developed to simulate PTSC performance. The study is being carried out in the locality of Birao in the Central African Republic (CAR).

2. Description model and mathematical formulation

The PTSC considered in this study is shown from its physical model in Figs. 1 and 2, with its main components such as the collector, absorber tube, glass envelope and metal support bracket. The system is equipped with a single-axis sun-tracking mechanism to maximize the collection and concentration of the sun's rays in order to obtain a good useable temperature. The end losses at the ends of the absorber tube shown in Fig. 2 are taken into account in the optical model. The technical dimensions, optical and thermal characteristics of PTSC are given in **Table A**.

The mathematically validated PTSC model from Ref. [33] is used in this study with different HTF configurations. Al_2O_3 and SiO_2 nanoparticles, being the most widely used in the literature according to Ref. [9], are selected and combined with vegetable oils to obtain nanofluids. Their thermophysical properties are taken from Table 1. Six HTF configurations are obtained, including two simple HTFs as base fluid (rapeseed and jatropha) and four nanofluid HTFs (Al_2O_3/rapeseed, SiO_2/rapeseed, Al_2O_3/jatropha, SiO_2/jatropha). The choice of rapeseed and jatropha was based on their compatibility with the nanoparticles selected according to the work of Ref. [12].

2.1. Energy modeling

In this section, the heat transfer equations defining the performance of the PTSC are presented. The energy flux received by the collector receiving surface is calculated from equation (1), where I_{beam} represents the direct solar irradiance in W/m^2, A_{col} the reflector area in m^2 [5].

$$Q_{solar} = I_{beam}A_{col} \tag{1}$$

The expression used to calculate the energy flow transmitted through the absorber tube to the HTF is given by equation (2).

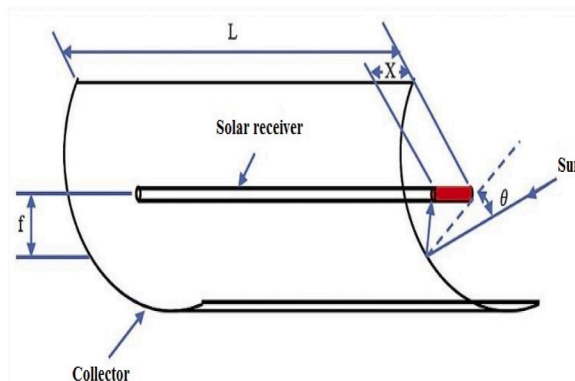$$Q_{useful} = \dot{m}C_{P,f}(T_{out} - T_{in}) \tag{2}$$

Fig. 2. End losses of heat collector element and geometry of collector [33].

Table 1

Thermophysical and rheological properties of base HTFs and nanoparticles.

Heat transfer fluid [32]	
Jatropha	Rapeseed
$k = 2.80 \times 10^{-7}T_f^2 - 2.258 \times 10^{-4}T_f + 0.1736$	$k = 2.10^{-7}T_f^2 - 1.714 \times 10^{-4}T_f + 0.1698$
$\nu = exp(4.5168 - 1.8371 \times \log(T_f))$	$\nu = exp(4.5966 - 1.7645 \times \log(T_f))$
$\rho = -0.6831T_f + 926.58$	$\rho = -0.6691 \times T_f + 928.19$
$C_p = 2.262 \times 10^{-9}T_f^4 - 10.423 \times 10^{-7}T_f^3 + 12.947 \times 10^{-5}T_f^2 + 0.441 \times 10^{-3}T_f + 1.9608$	$C_p = 1.621 \times 10^{-9}T_f^4 - 8.735 \times 10^{-7}T_f^3 + 14.933 \times 10^{-5}T_f^2 - 5.976 \times 10^{-3}T_f + 2.0985$
Nanoparticles [9,34–36]	
Al_2O_3	SiO_2
$k = 5.5 + 34.5 \times exp[-0.0033 \times (T_f - 273)]$	$k = 36$
$\rho = 3850$	$\rho = 3970$
$C_p = 1045 + 0.174 \times T_f - 2.80 \times 10^7 \times T_f^{-2}$	$C_p = 765$

In which $C_{p,f}$ is the heat capacity of HTF in J/kg.°C, the mass flow rate of HTF in kg/s. The outlet and inlet fluid temperatures are T_{out} and T_{in} in °C respectively.

The thermal efficiency from equations (1) and (2) can be calculated using the following expression is given by equation (3):

$$\eta_{thermal} = \frac{\int Q_{useful}dt}{\int Q_{solar}dt}$$

(3)

The various heat exchanges within the solar receiver are shown in Fig. 3, and its heat transfer modes according to the solar receiver compartments are described in Fig. 4 via the thermal resistance diagram. The temperature distribution of the absorber tube and fluid is derived from the overall heat balance obtained from the heat balance at the glass envelope, absorber tube and fluid levels using the first principle of thermodynamics. The various expressions used to calculate heat exchange are summarized in Table 2. Further information on modeling can be found in Ref. [33].

2.2. Thermophysical properties of nanofluids

The base fluids chosen have a temperature range of up to 250 °C, depending on the experimental conditions. Only the thermophysical properties of SiO_2 do not vary with temperature. The thermophysical properties of nanofluids can be determined experimentally or numerically. The numerical approach can be based either on energy equations or on correlations proposed in the literature. The numerical approach based on correlations is considered in this study. equations (4) and (5) for density and nanofluid specific heat respectively are given by Ref. [37]:

$$\rho_{nf} = \varphi\rho_{np} + (1 - \varphi)\rho_{bf}$$

(4)

$$C_{nf} = \frac{(1 - \varphi)(\rho C)_{bf} + \varphi(\rho C)_{np}}{(1 - \varphi)\rho_{bf} + \varphi\rho_{np}}$$

(5)

The thermal conductivity and viscosity of nanofluids are obtained from the following equations (6) and (7), respectively [38]:
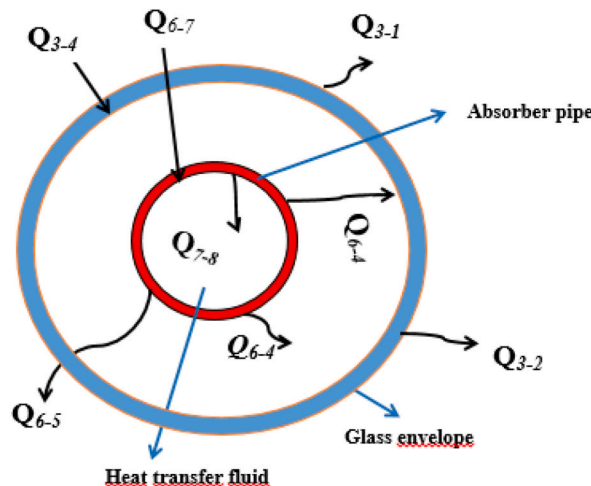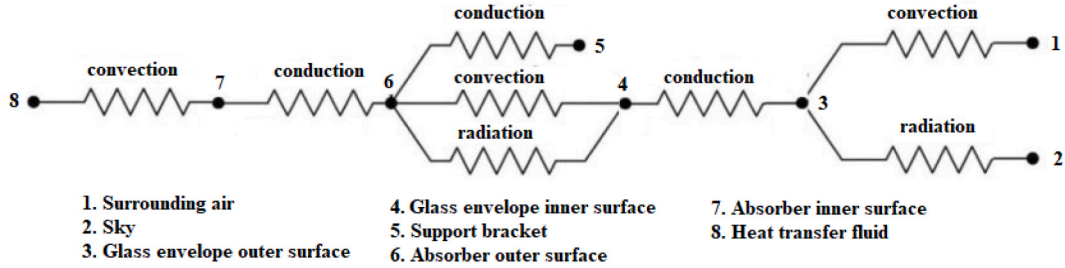

Fig. 3. Heat exchange balance.

Fig. 4. Overall thermal resistance scheme.

Table 2
Collector heat transfer models and heat transfer type.

	Heat transfer type	Heat transfer equation
3-2	Radiation	$Q_{3-2,rad} = \pi D_3 h_{3-2,rad}(T_e - T_s)$ $h_{3-2,rad} = \varepsilon_e \delta(T_s + T_e + 546)[(T_s + 273)^2 + (T_e + 273)^2]$ [19]
3-1	Convection	$Q_{3-1,conv} = \pi D_3 h_{3-1,conv}(T_e - T_a)$ $h_{3-1,conv} = \dfrac{k_3}{D_3} Nu_3$
3-4	Conduction	$Q_{3-4,dif} = \dfrac{\partial}{\partial x}\left(A_e k_e \dfrac{\partial T_e}{\partial x}\right)$
6-4	Convection	$Q_{6-4,conv} = \pi D_6 h_{6-4,conv}(T_{ab} - T_e)$ $h_{6-4,conv} = \dfrac{2}{D_6 \ln\left(\frac{D_4}{D_6}\right)}\left[0.386 k_a \left(\dfrac{Pr_a}{0.861 + Pr_a}\right)^{\frac{1}{4}}(Ra_c)^{\frac{1}{4}}\right]$ [19]
6-4	Radiation	$Q_{6-4,rad} = \pi D_6 h_{6-4,rad}(T_{ab} - T_e)$ $h_{6-4,rad} = \varepsilon_{ab}\delta(T_{ab} + T_e + 546)[(T_{ab} + 273)^2 + (T_e + 273)^2]$ [33]
6-5	Conduction	$Q_{6-5,cond} = h_{6-5,cond}(T_b - T_a)$ $h_{6-5,cond} = \sqrt{h_b k_b P_b A_{b,cs}}\tanh\left(\sqrt{\dfrac{h_b P_b}{k_b A_{b,cs}}}L_b\right)$ [41]
6-7	Conduction	$Q_{6-7,dif} = \dfrac{\partial}{\partial x}\left(A_{ab} k_{ab} \dfrac{\partial T_{ab}}{\partial x}\right)$
7-8	convection	$Q_{7-8,conv} = \pi D_8 h_{7-8,conv}(T_{ab} - T_f)$ $h_{7-8,conv} = \dfrac{k_f}{D_8} Nu_f$

$$k_{nf} = k_{bf}\frac{k_{np} + (n-1)k_{bf} + (n-1)\left(k_{np} - k_{bf}\right)\varphi}{k_{np} + (n-1)k_{bf} - \left(k_{np} - k_{bf}\right)\varphi} \qquad (6)$$

$$\mu_{nf} = \mu_{bf}\left(1 + 2.5\varphi + 6.5\varphi^2\right) \qquad (7)$$

In these equations, φ represents the volume fraction of the nanoparticle calculated from equation (8) [39]:

$$\varphi = \frac{\frac{\omega \rho_{bf}}{100}}{\left(1 - \frac{\omega}{100}\right)\rho_{np} + \frac{\omega}{100}\rho_{bf}} \qquad (8)$$

With subscripts np stands for nanoparticle, bf stands for base fluid and ω weight concentration in %, n is the empirical form factor given by n = 3/ψ with the denominator as the sphericity of the nanoparticle taken as 1.

2.3. Numerical solution procedure

In the simulation procedure, the Gauss-Seidel method is applied, based on a numerical code written in the Matlab software, with a convergence criterion set at 0.001 °C according to the literature [19,33]. Note that the simulation is carried out for each hour of the day. Other conditions or assumptions considered in this numerical simulation study are described in Ref. [33]. The flowchart followed in this study is shown in Fig. 5.

3. Results and discussion

In the validation of the numerical model, the operating conditions were determined by the experimental study in the literature. For the rest of the work, wind speed is assumed to average 2 m/s. A radiation estimation model is used, coupled to the PTSC optical model. Direct solar radiation varies as a function of local time, and an East-West tracking system with a North-South axis is used. The average optical efficiency is 70 %.

3.1. Numerical model validation

The numerical model and numerical simulation conditions are taken from Ref. [33]. In the lack of an experimental study carried out
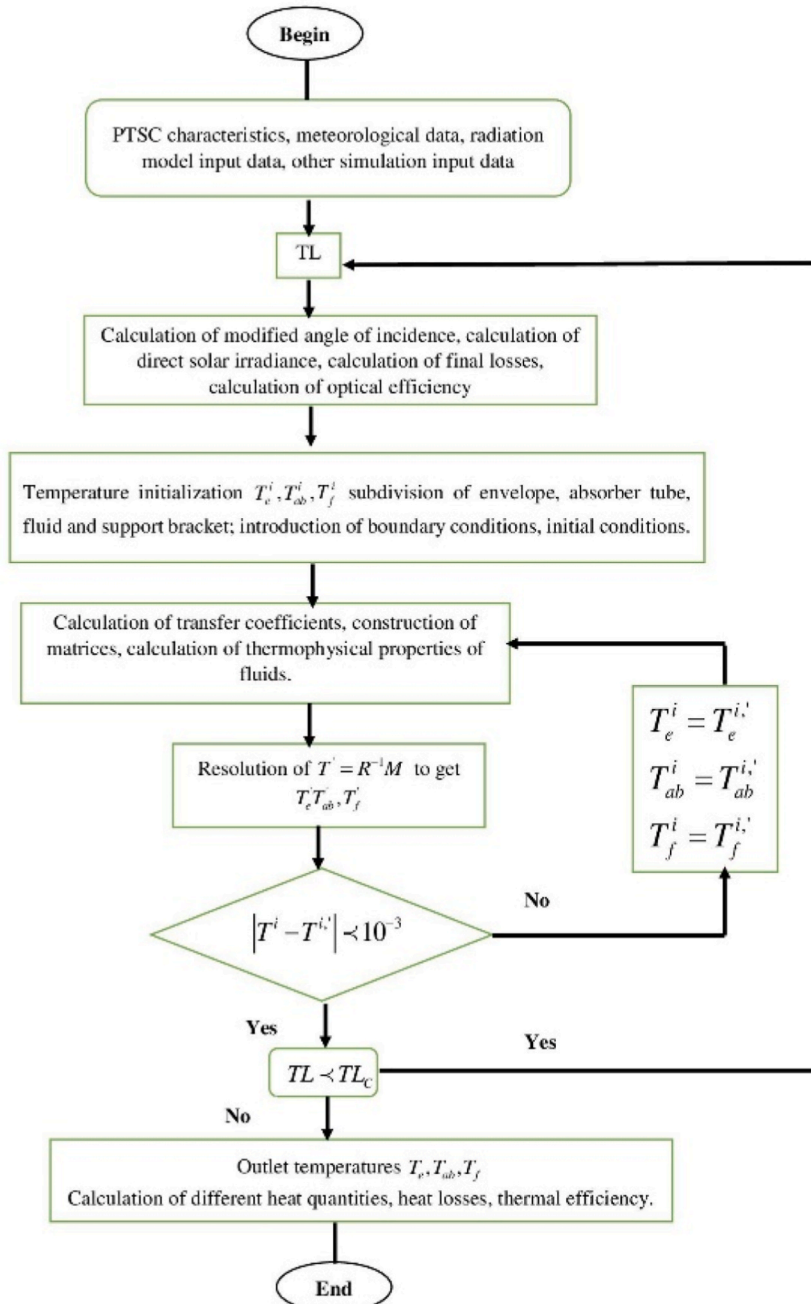

Fig. 5. Problem solving flowchart.

under the same conditions as this work, the experimental data of Ref. [40] are used for validation and then a comparison with those of Ref. [34]. Rapeseed oil and the nanofluids SiO_2/rapeseed, Al_2O_3/rapeseed are used as HTFs to simulate performance, and the volume fraction used is 3.5 %. The comparison is made in terms of thermal efficiencies. DNI, mass flow rate, wind speed, ambient temperature and fluid inlet temperature are the various input parameters for the four (4) tests (Table 3). From this, we can see differences in values between the current models, which are attributed to the differing contributions of the HTF configurations. The average deviation between the current and experimental models is 7.30 %, and 2.84 % with the model of Ref [34]. This can be justified by the operating conditions set during the experiment when characterizing the vegetable oil, which gave rise to the thermophysical and rheological properties at an operating temperature limited to 250 °C via the work of Ref. [12]. However, given the flash point temperature of 230 °C–330 °C, the vegetable oil could reach high temperatures close to those of the reference solar oil Therminol VP-1 and improve thermal performance under the required conditions of experiments to determine thermophysical and rheological properties. Also, based on the assumptions made in the numerical model of PTSC (consideration of end losses, addition of thermal effects of the support bracket, etc.) and the uncertainties in the measurements, the agreement between the experimental and the current model can be said to be good enough and sufficient to be able to use this approach in other simulations firstly from vegetable oils and secondly from nanofluids based on vegetable oils as HTFs in PTSC. In the following, comparative thermal analyses are made on the combined effects of the input parameters considered during the validation on the dynamic operation of the PTSC and also the variational effects of the nanoparticle concentration. In addition to the above HTFs, jatropha and SiO_2/jatropha, Al_2O_3/jatropha nanofluids are combined in the thermal analysis.

3.2. Dynamic effects of solar irradiance

PTSC operation depends on solar radiation, and its dynamics have variable effects on performance. For this analysis, six (6) HTF configurations are analyzed, the mass flow rate is assumed equal to 0.06 kg/s with a nanoparticle concentration of 3.5 %, the inlet fluid temperature is assumed fixed equal to 25 °C. Fig. 6 describes the effects of solar irradiance on the temperatures at the absorber tube outlet (Fig. 6a) and fluid outlet (Fig. 6b). The ununiformed temperature distribution at the absorber tube and HTFs is due to the non-uniform distribution of heat flux creating a temperature gradient. At the absorber tube level, this temperature gradient is influenced externally by the solar irradiance profile and internally by the heat transfer capacity of the fluid circulating inside. The impact differs from one HTF to another. Firstly, the temperature of rapeseed increases rapidly more than that of jatropha for time intervals of high solar irradiance. This shows how sensitive they are to variations in solar irradiance like most traditional fluids, in agreement with the results of Ray et al. [42] and Refs. [35,36]. The temperature gradient increases with solar irradiance, and the use of nanofluids reduces it. This reduces losses in the system, while increasing outlet temperatures. In this context, the best configurations are those based on Al_2O_3 nanofluids, which reach high temperatures at peak solar irradiance. Apart from the chemical characteristics and compositions of the base fluids, their combinations with Al_2O_3 nanoparticles have more positive effects on heat transfer performance than SiO_2, which can be justified by their thermophysical properties.

In view of these results and knowing the particularity of the use of nanoparticles which is to increase the capacity of the base fluid to transfer heat, a variation of the concentration of nanoparticles could have influence on the performances, being able to contribute to reduce the losses generated from the sources of irreversibility of the system.

3.3. Dual effects of nanoparticle volume concentration and solar irradiance on thermal performance

In this section, the dual effects of irradiance and nanoparticle volume fraction on the thermal behavior of the PTSC are evaluated. This evaluation is done in key hours (10 h–15 h) of the day when solar irradiance is high. The inlet fluid temperature is fixed at 25 °C and a mass flow rate of 0.06 kg/s. By varying the nanoparticle volume fraction from 1 % to 4 %, Table 4 provides information on the variation of the thermal efficiency of the PTSC system using the four nanofluids configurations. For the purpose of comparing the rate of efficiency improvement, the base fluids (rapeseed, jatropha) are also evaluated under the same operating conditions. For all HTFs, a general decrease in thermal efficiency can be observed from 10 h to 15 h local time, which can be explained by the progressive increase in heat losses within the system due to the increase in solar irradiance that creates thermal gradients. An increase in thermal efficiency on average of about 4.21 % is observed when using rapeseed compared to jatropha. For each set hour and each 1 % increase in nanoparticle concentration, the yield compared to the rapeseed base fluid on average increases by about 1.96 % when Al_2O_3/rapeseed nanofluid is used, and also by 0.47 % when SiO_2/rapeseed nanofluid is used. Also, for each hour of the fixed irradiance and for each 1 %

Table 3
Comparison of results from validation tests of the current model with those from Refs [34,40].

Run	I (W/ m^2)	flow rate (kg/s)	V$_{wind}$ (m/s)	Tair (°C)	T$_{in}$ (°C)	Eff$_{exp}$ (%) Ref [40]	Eff_0 (%)	Eff_1 (%)	Eff_2 (%)	Err_0 (%)	Err_1 (%)	Err _2 (%)	Err % Ref [34]
1	968.2	0.6522	3.7	22.4	151	70.9	67.112	67.218	67.113	5.34	5.19	5.35	6.35
2	982.3	0.6348	2.5	24.3	197.5	70.17	65.471	66.026	66.008	6.69	5.90	5.93	2.52
3	909.5	0.6596	3.3	25.6	250.7	70.25	62.837	63.111	63.1	10.55	10.16	10.17	7.32
4	937.9	0.6229	1.0	28.8	297.8	67.98	62.440	63.11	63.09	8.15	7.16	7.19	1.17
Mean										7.68	**7.10**	7.16	4.47

a) Absorber temperature
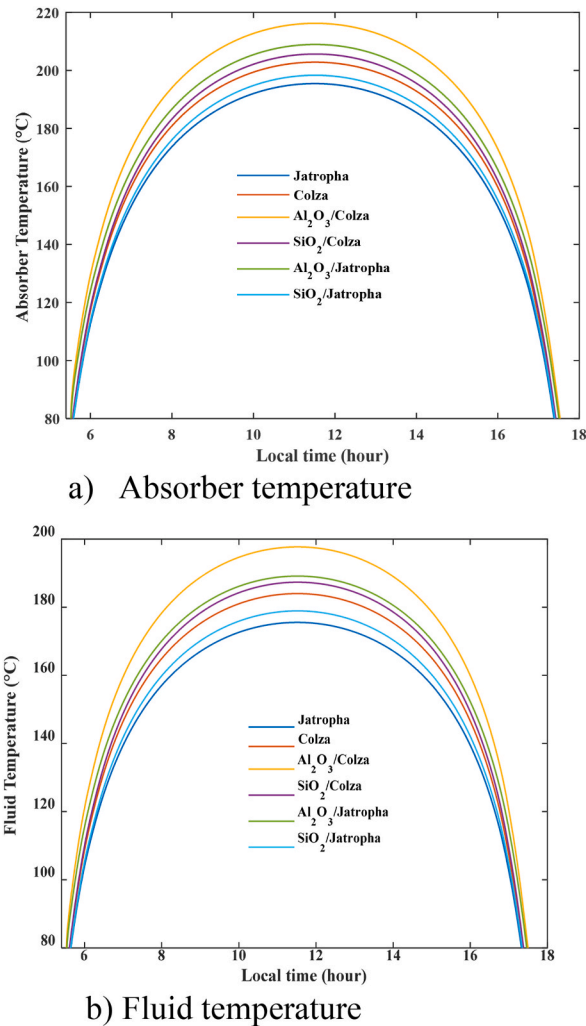

b) Fluid temperature

Fig. 6. Daily profile of absorber tube outlet temperatures and HTFs as a function of hourly irradiance.

increase in nanoparticle concentration, the thermal efficiency relative to the Jatropha base fluid on average increases by about 1.98 % when the Al_2O_3/Jatropha nanofluid is used and decreases by about 0.20 % on average when SiO_2/Jatropha is used. This negative effect of the SiO_2/Jatropha nanofluid on the thermal efficiency, in contrast to the other configurations presented, appears to be far removed from the results generally obtained in the case of traditional fluid-based nanofluids according to Ref. [11]. The generally expected impact was not observed. This could be attributed to the increase of the friction factor due to the dual effects that negatively influence the velocity and pressure inside the absorber tube thus generating the reduction of the global heat transfer coefficient which, in addition, reduces the mass heat capacity of the nanofluids. The increase of the concentration of nanoparticles leads to the reduction of the thermal capacity, which decreases with the thermal efficiency. Given the trend in Table 4, a low concentration of <0.1 % SiO_2 could lead to a higher thermal efficiency of SiO_2/Jatropha than the base fluid. This result shows that the use of nanoparticles with high thermal conductivity does not necessarily guarantee an increase in thermal efficiency but could rather reduce the performance for high nanoparticle concentration. Thus, only the positive effects of nanoparticles on the thermal conductivity of the nanofluids are not always sufficient in increasing the thermal performance, especially the thermal efficiency of a PTSC system and that the effects on the heat capacity should also be considered. This aspect was also emphasized by Mwesigye et al. [38], in the conclusion of their study with a traditional fluid. It can be concluded that the effect of solar irradiance influences more than that of nanoparticle concentration.

3.4. Dual effects of mass flow rate and nanoparticle concentration on thermal performance

In this section the dual effects concerning the mass flow rate and the volume concentration of the nanoparticles are investigated and recorded in Table 5 in order to see to what extent to propose an optimal configuration in agreement with the results of the previous section. This analysis was performed at 11:00 local time under fixed solar irradiance, with a range of nanoparticle concentration variation of 1–4% and for the mass flow rate of 0.06–0.46 kg/s. For all HTFs configurations, the thermal efficiency decreases with

Table 4

Comparison of the dual effects of solar irradiance and the variation of the nanoparticle concentration according to the HTFs configurations on the thermal efficiency of the PTSC (in %).

LOCALTIME	10 h				11 h				12 h				13 h				14 h				15 h			
VOLUME FRACTION	1 %	2 %	3 %	4 %	1 %	2 %	3 %	4 %	1 %	2 %	3 %	4 %	1 %	2 %	3 %	4 %	1 %	2 %	3 %	4 %	1 %	2 %	3 %	4 %
JATROPHA	69.84	69.84	69.84	69.84	70.04	70.04	70.04	70.04	70.18	70.18	70.18	70.18	70.28	70.28	70.28	70.28	70.38	70.38	70.38	70.38	70.55	70.55	70.55	70.55
COLZA	74.04	74.04	74.04	74.04	74.18	74.18	74.18	74.18	74.30	74.30	74.30	74.30	74.44	74.44	74.44	74.44	74.62	74.62	74.62	74.62	74.95	74.95	74.95	74.95
AL$_2$O$_3$/COLZA	76.02	77.99	79.93	81.84	76.12	78.05	79.96	81.84	76.24	78.16	80.06	81.94	76.39	78.33	80.25	82.14	76.63	78.62	80.58	82.51	77.08	79.18	81.25	83.28
SIO$_2$/COLZA	74.49	74.95	75.41	75.87	74.63	75.09	75.55	76.03	74.76	75.22	75.69	76.17	74.90	75.36	75.84	76.31	75.08	75.56	76.03	76.52	75.43	75.91	76.39	76.89
AL$_2$O$_3$/JATROPHA	71.80	73.74	75.66	77.55	71.96	73.87	75.76	77.62	72.09	73.99	75.88	77.73	72.21	74.13	76.03	77.90	72.36	74.33	76.27	78.19	72.64	74.71	76.76	78.77
SiO$_2$/JATROPHA	69.63	69.42	69.21	69.01	69.84	69.65	69.46	69.27	69.99	69.80	69.62	69.43	70.09	69.90	69.71	69.53	70.18	69.98	69.78	69.59	70.33	70.11	69.89	69.68

Table 5

Comparison of the dual effects of nanoparticle volume fraction and mass flow rate according to HTFs configurations on the thermal efficiency of the PTSC (in %).

LOCALTIME					11 h															
VOLUME FRACTION	1 %					2 %					3 %					4 %				
FLOW RATE (KG/S)	0.06	0.16	0.26	0.36	0.46	0.06	0.16	0.26	0.36	0.46	0.06	0.16	0.26	0.36	0.46	0.06	0.16	0.26	0.36	0.46
JATROPHA	65.75	60.12	54.02	48.25	42.55	65.75	60.12	54.02	48.25	42.55	65.75	60.12	54.02	48.25	42.55	65.75	60.12	54.02	48.25	42.55
COLZA	69.88	64.52	57.33	50.88	44.73	69.88	64.52	57.33	50.88	44.73	69.88	64.52	57.33	50.88	44.73	69.88	64.52	57.33	50.88	44.73
AL_2O_3/COLZA	71.81	69.22	63.75	58.60	53.53	73.74	74.05	70.55	66.99	63.29	75.64	78.93	77.63	75.95	73.94	77.52	83.80	84.86	85.28	85.25
SIO_2/COLZA	70.33	65.01	57.80	51.34	45.19	70.79	65.51	58.28	51.81	45.65	71.25	66.02	58.77	52.28	46.12	71.72	66.54	59.26	52.76	46.59
AL_2O_3/JATROPHA	67.66	64.39	59.89	55.39	50.74	69.57	68.77	66.07	63.10	59.79	71.45	73.22	72.51	71.30	69.61	73.31	77.67	79.09	79.82	79.99
SIO_2/JATROPHA	65.59	59.28	52.51	46.27	40.30	65.44	58.45	51.01	44.27	38.03	65.28	57.62	49.50	42.27	35.74	65.13	56.79	48.00	40.26	33.43

increasing mass flow rate and at the same time increases with volume fraction. An average decrease in efficiency of about 6 % is observed with each 0.1 kg/s increase in base fluid (rapeseed and jatropha). For volume fraction dependent HTFs configurations, the sensitivity of thermal efficiency to flow rate variation is implicitly a function of the nanoparticle configuration and its concentration. For the nanofluid configuration with SiO_2, at 1 % volume fraction, the thermal efficiency decreases by about 5.30 % on average with each 0.1 kg/s increase. This rate of gradual decrease in efficiency with respect to mass flow rate increases by about 1 % with each 1 %
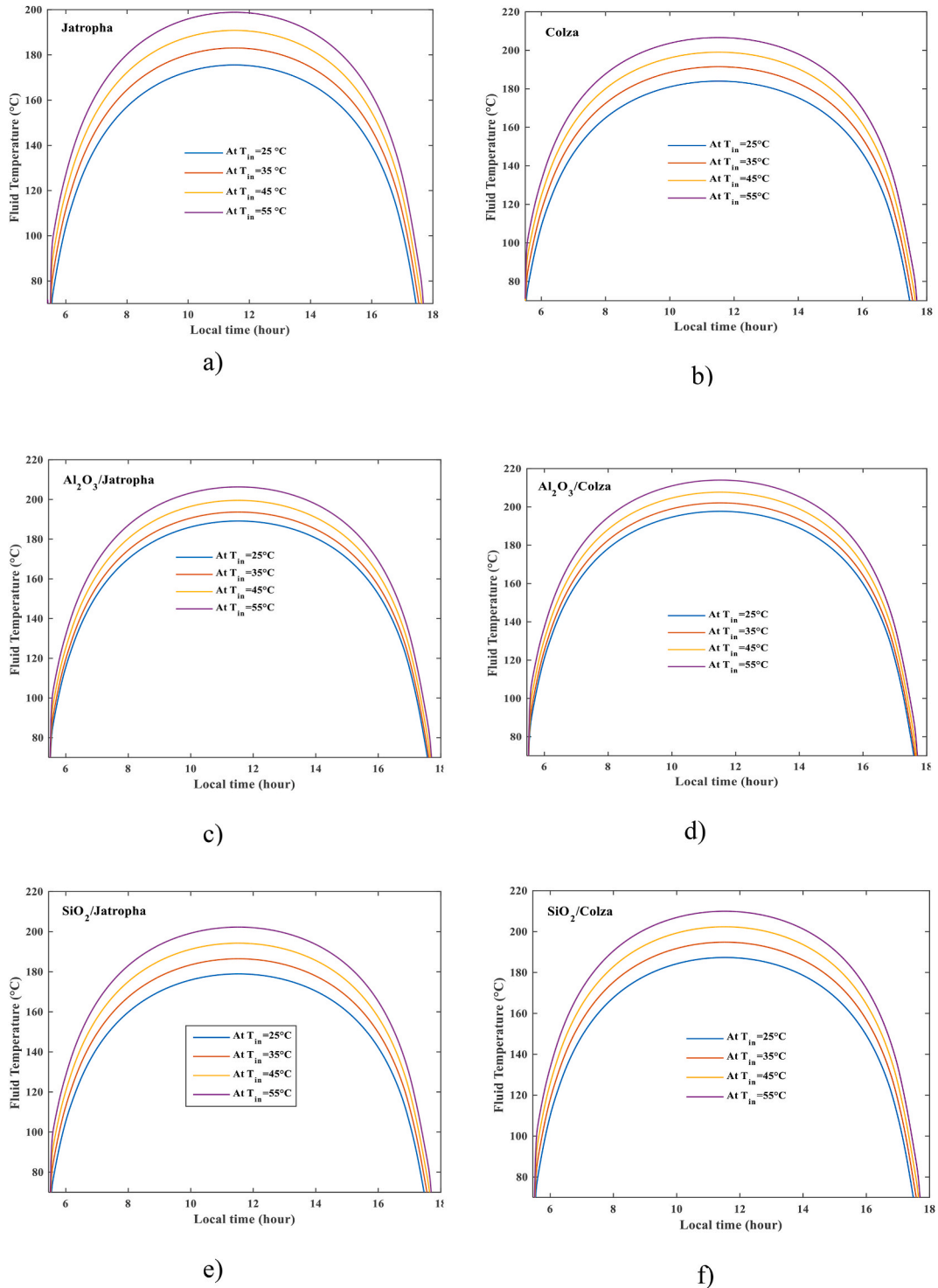

Fig. 7. Differential daily effects of HTF inlet temperatures on their outlet temperatures.

increase in volume fraction. For the nanofluids configuration with Al_2O_3, at 1 % volume fraction, the thermal efficiency decreases very variably with each 0.1 kg/s increase. The same is true when the rate of gradual decrease in efficiency versus mass flow rate increases with each 1 % increase in volume fraction. The best configurations of HTFs are Al_2O_3/rapeseed, SiO_2/rapeseed, and Al_2O_3/jatropha for nanoparticle volume fractions in the 3–4% range. As for the mass flow rate, the choice depends on the type of thermal performance sought (temperature or yield). For this work, the optimum chosen is 0.06 kg/s, volume fraction at 3.5 % and Al_2O_3/rapeseed nanofluid.

3.5. Effects of inlet fluid temperature on thermal performance

As presented by the experimental study [40], and in validation tests as a highly influential parameter, fluid inlet temperature plays a role in the energy transfer process in PTSCs [34]. This section describes the variational effects of fluid inlet temperature on PTSC system performance. The evaluation is first carried out on the fluid outlet temperature and then on the thermal efficiency of the system for each HTF configuration. For this analysis, the flow rate is set at 0.06 kg/s and the nanoparticle volume fraction at 3.5 %.

On HTF outlet temperature: Fig. 7a–f shows the results obtained for each HTF from the variation in inlet temperature over a range from 25 °C to 55 °C in 10 °C steps. For all the HTF configurations used, the outlet temperature increases with the inlet temperature, in accordance with the results of Ray et al. [43]. The increase in inlet fluid temperature is seen as a preheating system that promotes rapid temperature rise as the fluid flows through the absorber tube to reach high outlet temperatures. When the maximum temperature of the HTF is quickly reached at a distance $\Delta x < L$ of the length of the absorber tube before the end of the flow process, the temperature gradient (between the inner and outer surface of the absorber tube) created in the absorber tube favors the increase of heat losses. This depends strongly on the thermophysical and optical properties of the absorber tube. These effects are quantified at all temperatures, which can be seen in Figs. 8 and 9 from a comparison of the differences between the outlet temperature values of the absorber tube and the HTF depending on the configuration. All this generally affects the thermal efficiency of the system which is very sensitive to the variation of the thermal gradient. For each variation of the inlet temperature from 25 °C to 55 °C by steps of 10 °C, the average temperature during the day increases by about 5 °C using Al_2O_3/rapeseed, 8 °C using rapeseed, 7 °C using jatropha, 7.5 °C using SiO_2/rapeseed, 5 °C using Al_2O_3/jatropha and 7 °C using SiO_2/jatropha. This increase in inlet temperature is more favorable to the rapeseed fluid but the high temperatures are obtained using Al_2O_3/rapeseed.

On thermal efficiency: the thermal efficiency analyses of the PTSC system were evaluated between 10:00 and 14:00 local time and the results are recorded in Table 6. It can be seen that the thermal efficiency of all HTFs configurations decreases with increasing inlet fluid temperature. This result was found by Ray et al. [43] in their work. The influence is less observed during average sunshine hours. These effects are more important for nanofluids due to their high heat transfer capacity compared to base fluids.

Thus the choice of the inlet temperature of the fluid must take into account the amount of incoming heat flow in order to limit the thermal losses. The best thermal performance for all HTF configurations is obtained at 25 °C and the Al_2O_3/rapeseed nanofluids is the best HTF. Finding an optimal condition for best performance in both fluid outlet temperature and thermal efficiency of the PTSC would be an asset for its proper operation.

4. Conclusions

The quantitative and qualitative thermal analyses carried out in this study have led to several understandings of the proposed new thermal design. The PTSC model is validated with three HTFs configurations (rapeseed, Al_2O_3/rapeseed, SiO_2/rapeseed) in comparison with the numerical results of Ref [34] and experimental results of Ref [40] and an optimal PTSC approach is obtained. Based on the key parameters of the model used in its numerical validation and also on the different configurations of HTFs, several comparative studies of the different dual effects have been made and the main conclusions are as follows.
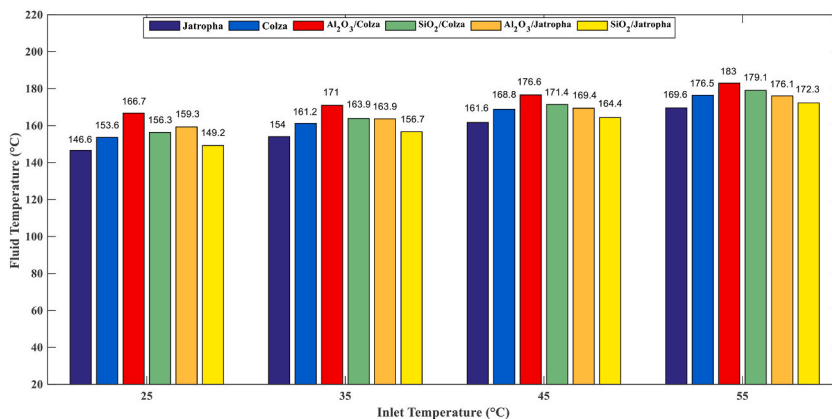

Fig. 8. Average effects of variable inlet temperatures of HTFs on their outlet temperatures.
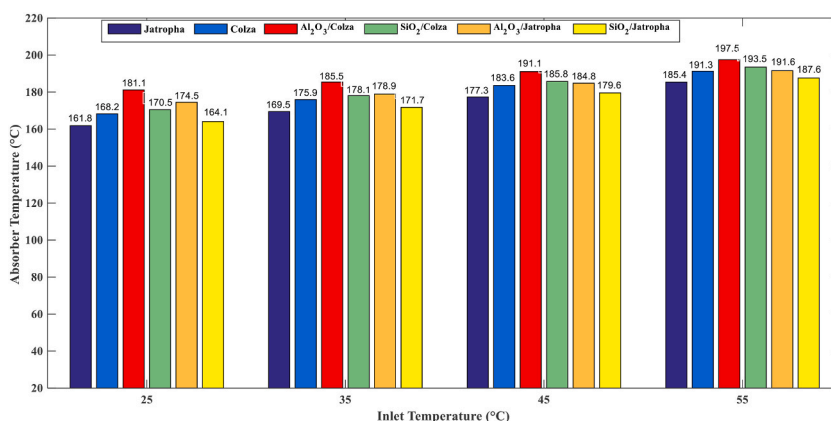
Fig. 9. Average effects of variable HTF inlet temperatures on the absorber tube outlet temperature according to configurations.

- The use of rapeseed increases the thermal efficiency of the system by around 4.21 % compared with Jatropha. The use of 1 % Al_2O_3 with rapeseed increases thermal efficiency by 1.96 %, while the use of 1 % SiO_2 with rapeseed improves thermal efficiency by 0.47 %. For both base fluids, on average Al_2O_3 improves the thermal efficiency of the PTSC more than SiO_2 by 1.97 % and less than 1 % respectively.
- Increasing the concentration of nanoparticles leads not only to improved performance, but also to a reduction in heat capacity, which decreases with thermal efficiency. However, the use of nanoparticles with high thermal conductivity does not necessarily guarantee an increase in the thermal efficiency of the PTSC system.
- Increasing the base fluids by 0.1 kg/s reduces thermal efficiency by an average of 6 %. The best configuration is Al_2O_3/rapeseed with 0.06 kg/s volume fraction 3.5 %.
- For a range from 25 to 55 °C, increasing the inlet fluid temperature by 10 °C improves the outlet temperature of base fluids (8 °C for rapeseed, 7 °C for jatropha), followed by nanofluids with SiO_2 (7.5 °C for SiO_2/rapeseed, 7 °C for SiO_2/jatropha) and then nanofluids with Al_2O_3 (5 °C for Al_2O_3/rapeseed and 5 °C for Al_2O_3/jatropha). However, high temperatures are obtained with Al_2O_3/rapeseed.

New experimental studies on the characterization and determination of the thermo-physical and rheological properties of vegetable oils under new operating conditions more improved than those of Ref [12,32] could be promising in exploiting their high-temperature properties. This would make vegetable oils better HTFs in PTSC compared with synthetics such as Therminol VP-1.

Funding statement

Data availability statement

The data used are included in the manuscript and the references have been mentioned in the manuscript.

CRediT authorship contribution statement

Venant Sorel Chara-Dackou: Writing – review & editing, Writing – original draft, Visualization, Validation, Software, Resources, Methodology, Investigation, Formal analysis, Data curation, Conceptualization. **Donatien Njomo:** Visualization, Validation, Supervision, Conceptualization. **René Tchinda:** Visualization, Validation, Supervision, Conceptualization. **Yvon Simplice Kondji:** Visualization, Validation, Supervision, Conceptualization. **Mahamat Hassane Babikir:** Writing – review & editing, Writing – original draft, Software, Methodology, Formal analysis, Conceptualization. **Hermann Chopkap Noume:** Software, Methodology, Formal analysis, Data curation. **Boris Abeli Pekarou Pemi:** Writing – original draft, Resources, Methodology, Formal analysis. **Armel Zambou Kenfack:** Software, Resources, Investigation, Formal analysis. **Ibrahim Ngapouth Mbouombouo:** Writing – review & editing, Visualization, Validation, Supervision, Resources.

Declaration of competing interest

The authors declare that this study has in no way been funded by any company or institution. It is the personal contribution of the paper authors.

Table 6

Comparison of the dual effects of solar irradiance and inlet temperature according to HTF configurations on the thermal efficiency of the PTSC (in %).

	10 h				11 h				12 h				13 h				14 h			
INLET TEMPERATURE	**25°C**	**35°C**	**45°C**	**55°C**	**25°C**	**35°C**	**45°C**	**55°C**	**25°C**	**35°C**	**45°C**	**55°C**	**25°C**	**35°C**	**45°C**	**55°C**	**25°C**	**35°C**	**45°C**	**55°C**
JATROPHA	70.04	69.03	68.12	67.34	70.18	69.18	68.28	67.50	70.28	69.28	68.36	67.57	70.38	69.35	68.41	67.58	70.55	69.48	68.49	67.60
COLZA	74.18	73.14	72.13	71.19	74.30	73.27	72.27	71.34	74.44	73.40	72.38	71.44	74.62	73.56	72.51	71.51	74.95	73.87	72.76	71.69
AL_2O_3/COLZA	80.90	78.35	76.43	74.92	81.01	78.48	76.58	75.09	81.20	78.64	76.72	75.20	81.55	78.90	76.90	75.30	82.27	79.45	77.29	75.56
SIO2/COLZA	75.79	74.75	73.75	72.83	75.93	74.90	73.91	73.01	76.07	75.04	74.03	73.11	76.27	75.21	74.16	73.18	76.64	75.54	74.43	73.36
AL_2O_3/JATROPHA	76.69	74.19	72.37	71.01	76.81	74.33	72.53	71.19	76.97	74.46	72.64	71.28	77.24	74.64	72.75	71.32	77.77	75.00	72.98	71.43
SIO_2/JATROPHA	69.36	68.46	67.65	66.96	69.52	68.63	67.82	67.14	69.62	68.72	67.90	67.21	69.69	68.76	67.92	67.19	69.78	68.83	67.94	67.15

Annexe.

Table A
PTSC technical specifications [19].

Parameter	Value/unit
Absorber length (L)	7.8 m
Concentrator aperture (w_{ap})	5 m
Focal length (f)	1.84 m
Concentration factor	22.42
Aperture angle ($\varnothing$)	68.38°
Absorber outer diameter (D_6)	0.07 m
Absorber inner diameter (D_7)	0.066 m
Glass envelope outer diameter (D_4)	0.115 m
Glass envelope inlet diameter (D_3)	0.109 m
Absorber thermal conductivity (k_{ab})	54 W/m°C
Glass envelope thermal conductivity (k_e)	1.2 W/m°C
Absorber tube absorption (α_{ab})	0.906
Glass envelope absorption (α_e)	0.02
Glass envelope transmitivity (τ_e)	0.95
Transmitivity-absorptivity factor (α_0)	0.864
Absorber thermal capacity (Cp_{ab})	500 J/kg°C
Glass envelope thermal capacity (C_{pe})	1090 J/kg°C
Absorber density (ρ_{ab})	8020 kg/m^3
Glass envelope density (ρ_e)	2230 kg/m^3
Absorber emissivity (ε_{ab})	0.14
Glass envelope emissivity (ε_e)	0.86
Reflectance of reflector (ρ_0)	0.93
Interception factor (γ)	0.92

References

[1] A.M. Ekoe A Akata, D. Njomo, B. Agrawal, A. Mackpayen, A.-H.M. Ali, Tilt Angle and Orientation assessment of photovoltaic thermal (PVT) system for Sub-Saharan Tropical Regions: case study Douala, Cameroon, Sustainability 14 (2022) 15591, https://doi.org/10.3390/su142315591.

[2] Djeudjo Temene Hermann, Njomo Donatien, Talla Konchou Franck Armel, Tchinda René, Techno-economic and environmental feasibility study with demand-side management of photovoltaic/wind/hydroelectricity/battery/diesel: a case study in Sub-Saharan Africa, Energy Convers. Manag. 258 (2022), https://doi.org/10.1016/j.enconman.2022.115494.

[3] V.S. Chara-Dackou, D. Njomo, M.H. Babikir, I.N. Mbouombouo, A.S. Pofoura Gboulie, R. Tchinda, Processing sunshine Duration measurements for the assessment of solar radiation in climatic Regions of the Central African Republic, J. Solar Energy Engin. June 144 (2022) 1–15, https://doi.org/10.1115/1.4053483 (15 pages).

[4] Sandro Ni_zetic, Nedjib Djilali, Agis Papadopoulos, J. Joel, P.C. Rodrigues, Smart technologies for promotion of energy efficiency, utilization of sustainable resources and waste management, J. Clean. Prod. 231 (2019) 565e591, https://doi.org/10.1016/j.jclepro.2019.04.397.

[5] M.H. Babikir, V.S. Chara-Dackou, D. Njomo, M. Barka, M.Y. Khayal, D.R. Kamta Legue, J.P. Gram-Shou, Simplified modeling and simulation of electricity production from a dish/stirling system, Int. J. Photoenergy (2020), https://doi.org/10.1155/2020/7398496. Article ID 7398496, 14 pages.

[6] Cağatay Iris, Jasmine Siu Lee Lam, A review of energy efficiency in ports: operational strategies, technologies and energy management systems, Renew. Sustain. Energy Rev. 112 (2019) 170–182, https://doi.org/10.1016/j.rser.2019.04.069.

[7] Fuqiang Wang, Ziminga Cheng, Jianyu Tan, Yuan Yuan, Yong Shuai, Linhua Liu, Progress in concentrated solar power technology with parabolic trough collector system: a comprehensive review, Renew. Sustain. Energy Rev. 79 (2017) 1314–1328, https://doi.org/10.1016/j.rser.2017.05.174.

[8] V.K. Jebasingh, G.M. Joselin Herbert, A review of solar parabolic trough collector, Renew. Sustain. Energy Rev. 54 (2016) 1085–1091, https://doi.org/10.1016/j.rser.2015.10.043.

[9] H. Olia, M. Torabi, M. Bahiraei, M.H. Ahmadi, M. Goodarzi, M.R. Safaei, Application of nanofluids in thermal performance enhancement of Parabolic Trough Solar collector: state-of-the-art, Appl. Sci. 9 (2019) 463, https://doi.org/10.3390/app9030463.

[10] Y. Krishna, M. Faizal, R. Saidur, K.C. Ng, N. Aslfattahi, State-of-the-art heat transfer fluids for parabolic trough collector, Int. J. Heat Mass Tran. 152 (2020) 119541, https://doi.org/10.1016/j.ijheatmasstransfer.2020.119541.

[11] MV Bindu and GMJ Herbert. A review on application of nanomaterials in heat transfer fluid for parabolic trough concentrator, Mater. Today: Proc., https://doi.org/10.1016/j.matpr.2021.01.957.

[12] J.-F. Hoffmann, Stockage thermique pour centrale solaire thermodynamique à concentration mettant en œuvre des matériaux naturels ou recyclés, Thèse de Doctorat à Universite De Perpignan Via Domitia, Décembre 2015, 2015.

[13] S.D. Odeh, G.L. Morrison, M. Behnia, Modelling of parabolic trough direct steam generation solar collectors, Sol. Energy 62 (6) (1998) 395–406.

[14] R.E. Forristall, Heat Transfer Analysis and Modeling of a Parabolic Trough Solar Receiver Implemented in Engineering Equation Solver, National Renewable Energy Laboratory, Golden, CO, 2003 (Internet resource).

[15] M.J. Montes, A. Aba_nades, J.M. Marti_nez-Val, Thermofluidynamic model and comparative analysis of parabolic trough collectors using oil, water/steam, or molten salt as heat transfer fluids, J. Sol. Energy Eng. 132 (2) (2010) 21001.

[16] M. Ouagued, A. Khellaf, Simulation of the temperature and heat gain by solar parabolic trough collector in Algeria, Int J Math Comput Phys Electr Comput Eng 6 (7) (2012) 746–752.

[17] Y. Wang, Q. Liu, J. Lei, H. Jin, A three-dimensional simulation of a parabolic trough solar collector system using molten salt as heat transfer fluid, Appl. Therm. Eng. 70 (1) (2014) 462–476.

[18] Reda Tahtah, Bouchoucha Ali, Cherifa Abid, Mahfoud Kadja, Fouzia Benkafada, Experimental Study of Heat Transfer in Parabolic Trough Solar Receiver: Using Two Different Heat Transfer Fluids, 2017.

[19] M.H. Babikir, D. Njomo, M. Barka, V.S. Chara-Dackou, Y.S. Kondji, M.Y. Khayal, Thermal modeling of a parabolic trough collector in a quasi-steady state regime, J. Renew. Sustain. Energy 13 (2021) 013703, https://doi.org/10.1063/1.5145272.

[20] G.K. Manikandan, S. Iniyan, Ranko Goic, Enhancing the optical and thermal efficiency of a parabolic trough collector–A review, Appl. Energy 235 (2019) 1524–1540, https://doi.org/10.1016/j.apenergy.2018.11.048.

[21] T. Sokhansefat, A.B. Kasaeian, F. Kowsary, Heat transfer enhancement in parabolic trough collector tube using Al2O3 synthetic oil nanofluid, Renew. Sustain. Energy Rev. 33 (2014) 636–644.

[22] T.C. Paul, A.K.M.M. Morshed, E.B. Fox, J.A. Khan, Thermal performance of Al2O3 nanoparticle enhanced ionic liquids (Neils) for concentrated solar power (CSP) applications, Int. J. Heat Mass Tran. 85 (2015) 585–594.

[23] A. Mwesigye, Z. Huan, J.P. Meyer, Thermodynamic optimization of the performance of a parabolic trough receiver using synthetic oil-Al2O3 nanofluid, Appl. Energy 156 (2015) 398–412.

[24] S. Toghyani, E. Baniasadi, E. Afshari, Thermodynamic analysis and optimization of an integrated Rankine power cycle and Nano-fluid based parabolic trough solar collector, Energy Convers. Manag. 121 (2016) 93–104.

[25] S.E. Ghasemi, A.A. Ranjbar, Thermal performance analysis of solar parabolic trough collector using nanofluid as working fluid: a CFD modelling study, J. Mol. Liq. 222 (2016) 159–166.

[26] M. Faizal, R. Saidur, S. Mekhilef, M.A. Alim, Energy, economic and environmental analysis of metal oxides nanofluid for flat-plate solar collector, Energy Convers. Manag. 76 (2013) 162–168, https://doi.org/10.1016/j.enconman.2013.07.038.

[27] Ashok K. Barok, Prasanta K. Satapathy, Sudhansu S. Sahoo, CFD study of forced convective heat transfer enhancement in a 90° bend duct of square cross section using nanofluid, Sadhana 41 (2016) 795–804, https://doi.org/10.1007/s12046-016-0507-6AbedN. Afgan, 2020 Afgan I. An extensive review of various technologies for enhancing the thermal and optical performances of parabolic trough collectors. Int J Energy Res. 2020; 1–46.

[28] Asish Sarangi, Abhisek Sarangi, Sudhansu Sekhar Sahoo, Ramesh Kumar Mallik, Subhankar Ray, Shinu M. Varghese, A review of different working fluids used in the receiver tube of parabolic trough solar collector, J. Therm. Anal. Calorim. 148 (2023) 3929–3954, https://doi.org/10.1007/s10973-023-11991-y.

[29] Chakraborty Oveepsa, Das Biplab, Rajat Gupta, Performance of parabolic trough collector with spinning star inserts in receiver tube with hybrid nanofluid, Proc. IME E J. Process Mech. Eng. (2023). https://doi.org/10.1177/09544089231158.

[30] Oveepsa Chakraborty, Biplab Das, Rajat Gupta, Thermal Performance Evaluation of Parabolic Trough Collector Having Different Inserts and Working with Hybrid Nanofluid, Energy & Environment, 2023, https://doi.org/10.1177/0958305X231156407.

[31] Oveepsa Chakraborty, Biplab Das, Rajat Gupta, Performance of parabolic trough collector having rotating receiver: effect of elliptical insert and hybrid nanofluid, Int. J. Energy Res. 46 (11) (2022) 15254–15275, https://doi.org/10.1002/er.8225.

[32] J.-F. Hoffmann, G. Vaitilingom, J.-F. Henry, M. Chirtoc, R. Olives, V. Goetz, X. Py, Temperature dependence of thermophysical and rheological properties of seven vegetable oils in view of their use as heat transfer fluids in concentrated solar plants, Sol. Energy Mater. Sol. Cell. 178 (2018) 129–138, https://doi.org/10.1016/j.solmat.2017.12.037.

[33] V.S. Chara-Dackou, D. Njomo, R. Tchinda, M.H. Babikir, Y.S. Kondji, Thermal performance analysis of the parabolic trough solar collector in the Sub-Saharan climate of the Central African Republic, Sustain. Energy Technol. Assessments 58 (2023) (2023) 103331, https://doi.org/10.1016/j.seta.2023.103331.

[34] E. Kaloudis, E. Papanicolaou, V. Belessiotis, Numerical simulations of a parabolic trough solar collector with nanofluid using a two-phase model, Renew. Energy 97 (2016) (2016) 218e229, https://doi.org/10.1016/j.renene.2016.05.046.

[35] Y.J. Wang, Q.B. Liu, J. Lei, H.G. Jin, Performance analysis of a parabolic trough solar collector with non-uniform solar flux conditions, Int. J. Heat Mass Tran. (2015) 236–249.

[36] Yanjuan Wang, Jinliang Xu, Qibin Liu, Yuanyuan Chen, Huan Liu, Performance analysis of a parabolic trough solar collector using Al2O3/synthetic oil nanofluid, Appl. Therm. Eng. 107 (2016) (2016) 469–478, https://doi.org/10.1016/j.applthermaleng.2016.06.170.

[37] Muhammad Sajid Khan, Mi Yan, Hafiz Muhammad Ali, Khuram Pervez Amber, Muhammad Anser Bashir, Bilal Akbar, Samina Javed, Comparative performance assessment of different absorber tube geometries for parabolic trough solar collector using nanofluid, J. Therm. Anal. Calorim. 142 (2020) 2227–2241, https://doi.org/10.1007/s10973-020-09590-2.

[38] Majid Moosavi, Elaheh K. Goharshadi, Abbas Youssefi, Fabrication, characterization, and measurement of some physicochemical properties of ZnO nanofluides, Int. J. Heat Fluid Flow 31 (2010) 599–605, 10.1016/j.ijheatfluidflow.2010.01.011.

[39] W.H. Azmi, K.V. Sharma, P.K. Sarma, Rizalman Mamat, Shahrani Anuar, V. Dharma Rao, Experimental determination of turbulent forced convection heat transfer and friction factor with SiO2 nanofluid, Exp. Therm. Fluid Sci. 51 (2013) 103–111, https://doi.org/10.1016/j.expthermflusci.2013.07.006.

[40] V. Dudley, G. Kolb, M. Sloan, D. Kearney, SEGS LS2 Solar Collector Test Results, Report of Sandia National Laboratories, 1994. Report No. SANDIA94e1884.

[41] H. Liang, S. You, H. Zhang, Comparison of different heat transfer models for parabolic trough solar Collectors, Appl. Energy 148 (2015) 105–114, https://doi.org/10.1016/j.apenergy.2015.03.059.

[42] Subhankar Ray, Arun Kumar Tripathy, Sudhansu S. Sahoo, Hitesh Bindra, Performance analysis of receiver of parabolic trough solar collector: effect of selective coating, vacuum and semitransparent glass cover, Int. J. Energy Res. 42 (13) (2018) 4235–4249, https://doi.org/10.1002/er.4137.

[43] Subhankar Ray, Arun Kumar Tripathy, Sudhansu S. Sahoo, Suneet Singh, Effec of inlet temperature of heat transfer fluid and wind velocity on the performance of parabolic trough solar collector receiver: a computational study, International journal of heat and technology 37 (No 1) (2019) 48–58, https://doi.org/10.18280/ijht.370106. March 2019.

Nomenclature

Abbreviations
PTSC: Parabolic Trough Solar Collector
HTF: Heat Transfer Fluid
CAR: Central African Republic

Symbols
A: surface (m^2)
C_p, C: specific heat at constant pressure (J/kg. °C)
D: diameter (m)
Eff: Efficiency (%)
Err: Error (%)
h: heat coefficient transfer (W/m^2.°C)
I: solar irradiance (Wh/m^2)
k: thermal conductivity (W/m. °C)
Q: heat (Wh)
ṁ: mass flow rate (kg/s)
T: temperature (°C)
TL_C: sunset time
TL: Local time

V: speed (m/s)
ṁ: mass flow rate (kg/s)
n: factor of empirical form

Greek symbols

φ: Volume fraction (%)
μ: dynamic viscosity (Pa.s)
ρ: density (kg/m^3)
η: Efficiency (%)
ε :: emissivity

Sucbsripts

a: surrounding air
ab: absorber
b: bracket
in: intlet
beam: beam radiation
co: collector
e: glass envelope
f: fluid
nf: nanofluid
bf: basefluid
np: nanoparticle
out: outlet
s: sky